Chemical and microscopic analysis of graphene prepared by different reduction degrees of graphene oxide

P. Solís-Fernández, R. Rozada*, J.I. Paredes, S. Villar-Rodil, M.J. Fernández-Merino, L. Guardia, A. Martínez-Alonso, J.M.D. Tascón

Instituto Nacional del Carbón, INCAR-CSIC, Apartado 73, 33080 Oviedo, Spain

*Corresponding Author: Email address: rozada@incar.csic.es. Telephone number: (+34) 985 11 90 90. Fax number: (+34) 985 29 76 62.

Abstract

Chemical reduction of exfoliated graphite oxide (graphene oxide) has become one of the most promising routes for the mass production of graphene sheets. Nonetheless, the material obtained by this method exhibits considerable structural disorder and residual oxygen groups, and reports on their microscopic structure are quite scarce. We have investigated the structure and chemistry of graphene oxide samples reduced to different degrees using atomic force and scanning tunneling microscopy (AFM/STM) as well as X-ray photoelectron spectroscopy (XPS) and temperature-programmed desorption (TPD), respectively. TPD and XPS results indicate that reduction proceeds mainly by eliminating the most labile oxygen groups, which are ascribed to epoxides and hydroxyls on basal positions of the graphene plane. AFM/STM shows that the sheets are composed of buckled oxidized regions intermingled with flatter, non-oxidized ones, with the relative area of the latter increasing with the reduction degree.

Keywords: graphene oxide; reduction; temperature-programmed desorption; scanning tunneling microscopy; atomic force microscopy

1. Introduction

Since it was first isolated in 2004, graphene, a two dimensional hexagonal network of carbon atoms, has grown in popularity within the scientific community due to its outstanding properties, which make it a potential candidate in many technological applications [1, 2]. Achieving the practical implementation of graphene on a large scale will rely on finding feasible approaches for the mass production and processing of this material. In this regard, chemical reduction of exfoliated graphite oxide (graphene oxide) appears to be one of the most convenient routes for graphene production available at present, providing great quantities of material in the liquid phase [3, 4]. However, the material obtained by this

method differs chemically and structurally from pristine graphene obtained, e.g., by micromechanical cleavage of graphite [5]. In particular, its characteristics strongly depend on the extent of reduction achieved [6-8]. Here we have investigated the chemical and morphological evolution of graphene oxide (GO) sheets with different reduction degrees using X-ray photoelectron spectroscopy (XPS) and temperature-programmed desorption (TPD), which are useful techniques to provide relevant chemical information of carbon materials [9-12] , and atomic force and scanning tunneling microscopies (AFM/STM), which allow imaging this type of graphene on the nanometer and atomic scales.

2. Materials and Methods

Graphene oxide sheets were obtained in the form of aqueous dispersions (0.1 mg mL^{-1}) from graphite oxide on the basis of previously reported procedures [5, 13]. Reduced graphene oxide (RGO) with different degrees of deoxygenation was prepared as follows [8]: highly reduced samples were made by heating the suspension at 95 ºC for 1h in the presence of 2 mM vitamin C (sample RGO-V), or 21 mM hydrazine (sample RGO-H) as a reductant; intermediate deoxygenation was achieved by the same procedure except for the use of 1 mM pyrogallol as a reducing agent (RGO-P); finally, mild deoxygenation was accomplished just in basic medium in the absence of any reductant. In the latter case, the suspensions were heated at 95 ºC for 4 h in the presence of 26 mM (sample RGO-N1) and 206 mM (sample RGO-N2) of ammonia. The choice of these reducing agents and conditions has been made on the basis of previous experimental observations [8], which afford covering a wide range of reduction degrees. In particular, the efficiency of reduction depends on the nature of the reducing reagent, although the reason behind such differences is not currently known.

XPS was performed on a SPECS system at 10^{-7} Pa with a monochromatic Al K_α X-ray source at 100 W. The surface charging effect in GO was counteracted by the use of an electron flood gun operated at 0.4 eV and 0.10 mA. TPD analysis of the samples was conducted in a Micromeritics Autochem II chemisorption analyzer with a heating rate of 10º C min^{-1} under flowing argon (50 mL min^{-1}). The amounts of released H_2O, CO and CO_2 were determined from the intensities of m/Z=18, 28, and 44, respectively, monitored by an Omnistar mass spectrometer (Pfeiffer Vacuum). Raman spectra were recorded with a Horiba Jobin-Yvon LabRam instrument at a laser excitation wavelength of 532 nm. AFM and STM investigations were conducted on a Nanoscope IIIa Multimode apparatus (Veeco Instruments) working under ambient conditions. The samples were prepared by drop-casting a small volume of diluted dispersion (5 μL, 0.01 mg mL^{-1}) onto a preheated (~50-60 ºC) highly oriented pyrolytic graphite (HOPG) substrate and allowing it to dry. STM imaging was accomplished in the constant current mode (variable height) with mechanically prepared Pt/Ir (80/20) tips. AFM was carried out in the tapping mode of operation, employing rectangular Si cantilevers with nominal spring constant and resonance frequency of ~40 N m^{-1} and ~250-300 kHz respectively. The electrical conductivity of thin RGO films prepared by vacuum filtration of the different reduced suspensions was evaluated by measuring the resistance of rectangular strips with a Fluke 45 digital multimeter. The film thickness was estimated by scanning electron microscopy.

3. Results and Discussion

The oxygen functionalities present in GO sheets transform much of the originally sp^2-hybridized carbon atoms of the graphene lattice to a sp^3-hybridized state, thus decreasing dramatically the electronic conjugation of the sheets and therefore their electrical conductivity. As reduction of GO proceeds and its oxygen-containing groups are removed,

sp^2 bonding and electronic conjugation are progressively restored, and therefore electrical conductivity increases. As a matter of fact, it has been shown that this property is highly sensitive to the reduction degree attained for GO [7]. In our case, the electrical conductivity measured for samples RGO-N1, RGO-N2, RGO-P, RGO-V and RGO-H was 0.05, 0.32, 488, 7700 and 9660 S m^{-1}, respectively, suggesting their reduction degree to be in the same order.

To follow the chemical evolution of GO upon reduction, XPS and TPD analyses were performed. Table 1 shows O/C and N/C atomic ratios for the investigated samples. The aforementioned order in the reduction degree of the samples is confirmed by the decreasing O/C ratio in the series. A minor amount of nitrogen is introduced in every sample, which must be related to the used base (NH_3) and/or the reducing agent. Fig. 1 shows high resolution C1s (a) and O1s (b-d) core level XPS spectra of some selected samples: GO (green), RGO-N1 (blue), and RGO-V (red). Samples RGO-N2, RGO-P and RGO-H (not shown) yielded results that are consistent with their reduction degree. The C1s band of GO consists of three components, assigned to carbons in unoxidized, aromatic sp^2 structures (binding energy of 284.6 eV), carbons singly bonded to oxygen (e. g. in hydroxyl and epoxy groups) and also possibly C-C bonds in defect structures (286.6 eV) [11], and carbon doubly bonded to oxygen (287.9 eV) [12]. From the relative intensity of such components, it is clear that oxygen groups present in GO are mainly epoxies and hydroxyls, both located in basal plane sites [14, 15]. Upon reduction, there is a notable drop in the intensity of the component associated to these basal plane groups (286.6 eV). For the more extensively reduced samples (RGO-V and RGO-H) the restoration of electronic conjugation is confirmed by the appearance of a $\pi \rightarrow \pi^*$ band at ~291.1 eV [11] (see inset of Fig 1a, where the ordinate scale of the spectra has been magnified). In the case of thermal reduction of GO, the appearance of such band has been reported for annealing temperatures above 400 ºC [16]. The increase in the order and

homogeneity in the chemical environment of sp^2 carbon is reflected in the narrowing of the corresponding band, from a full width at half maximum of ~1.4 eV in GO to ~1.1 eV and ~0.8 eV for RGO-N1 and RGO-V, respectively.

The O1s band was peak-fitted into four components (Fig. 1 b-d), which were assigned to the following species [17, 18]: doubly bonded oxygen (~531.3 eV); singly bonded oxygen in alcohols, ethers, epoxides and peroxides (~532.4 eV); singly bonded oxygen in acids, esters, and hydroperoxides (~533.3 eV); and peroxyacid, peroxyester and/or charge effect (~534.8 eV). The intensity of the latter was almost zero in most cases. As already observed in the C1s band, the intensity of the component at ~532.4 eV, which involves basal plane epoxides and hydroxyls, drops significantly with the reduction degree. On the other hand, the intensity of the bands related to groups at the edges of the graphene sheets remains basically unaltered by the reduction process. This is in agreement with recent theoretical calculations on the reduction mechanism of GO, which predicted a higher difficulty in the removal of oxygen-containing groups located at edges compared to those located at the interior of the basal planes [19].

Fig. 2 shows H_2O, CO and CO_2 TPD profiles for GO, RGO-N1 and RGO-V samples and Table 1 displays the total amounts released of such species also for samples RGO-P and RGO-H. The results for GO are similar to those found in the literature (reported only in the temperature range below 300 ºC) in that H_2O, CO and CO_2 are the primary desorption products of GO and the three of them are released at the same temperature [16, 20]. Evolution of CO and CO_2 can be attributed to the presence of oxygenated functionalities in the sheets. Therefore, the observed diminution in the total amounts of CO and CO_2 evolved for reduced samples in comparison with those of GO (see Table 1) indicates a decrease in the overall

amount of such species following reduction, which is also in agreement with the drop in the O/C ratio deduced by XPS (see Table 1). The TPD profiles for GO reveal that there is a strong evolution of CO in a very narrow range of low temperatures (~160-190 ºC), which is quite unusual for carbon materials [9, 21], but agrees with previous reports on GO [16, 20]. As established from the XPS results, oxygen groups present in GO are mainly epoxies and hydroxyls (see Fig. 1a and b), both located in basal plane sites [14, 15]. These are expected to be much more labile and therefore evolve at lower temperatures than the typically edge-located functionalities of carbon materials. Furthermore, although only CO evolution would be expected for isolated epoxy and hydroxyl functionalities, the very high density of these types of oxygen functionality present in the starting GO sample [1, 4, 5] should also facilitate the release of CO_2, which is energetically favorable in comparison with CO. Thus, we ascribe the low temperature release of CO and also CO_2 to desorption of basal plane epoxides and hydroxyls.

For the reduced samples, there is a pronounced decrease in the lower temperature evolution of CO and CO_2, indicating that chemical reduction involves mainly the most labile groups. These results are in agreement with previous theoretical and experimental studies of chemical reduction [8, 19]. H_2O evolution for samples GO and RGO-N1 below ~150 ºC may be ascribed to desorption of physisorbed water molecules, while the observed release in the 175-200 ºC range could be due either to desorption of more strongly adsorbed water or, alternatively, to water molecules produced in dehydration processes (e.g., formed by reaction of two hydroxyls). H_2O evolution for samples reduced to a higher extent is much smaller, which is consistent with their considerable degree of reduction (relatively little evolution of CO and CO_2, high electrical conductivity, lower O/C atomic ratio) and its subsequent expected hydrophobicity.

For temperatures above ~500 ºC, the evolution of CO for GO is significantly larger than that of its reduced counterparts. This appears to contradict the fact that reduction mainly proceeds through elimination of the most labile groups. Previous studies on carbon materials have attributed the evolution of CO at these temperatures to the presence of ethers, carbonyls and phenol-type hydroxyls [9]. Furthermore, recent theoretical calculations have suggested that chemical reduction cannot remove these types of oxygen-containing groups [19], so they should be still present in the reduced samples. We interpret that the stable oxygenated species responsible for the considerable release of CO above 500 ºC in GO were not present in the original sample before the TPD experiment, but instead they were originated during such experiment at lower temperatures. It has been recently shown that thermal desorption of oxygen-containing functional groups from GO modifies the structure of the material, creating vacancies and small holes, and many of the remaining epoxide and hydroxyl groups can readily migrate to these defects and form more stable, edge-located functionalities [22]. Thus, epoxides could transform into carbonyls and ethers, and basal plane hydroxyls into phenol-type hydroxyls. For the reduced samples, the amount of labile oxygen groups is rather small (little evolution of CO and CO_2 at 160-190 ºC), so only a small amount of stable groups will be generated as a result of thermal evolution for the former, thus explaining the comparatively small amounts of CO released for these samples above 500 ºC.

Raman spectroscopy was employed in an attempt to gain some general structural information on the investigated materials. Fig. 3 shows normalized first and second order Raman spectra of GO, RGO-N1 and RGO-V. The first-order Raman spectrum of the materials under study is characterized by strong bands at ~1350 and ~1580 cm^{-1}, known as D and G bands, respectively. Defect-free graphite would only show the G band, as the D band corresponds to

a phonon mode whose intensity is strictly connected to the presence of six-fold aromatic rings close to local lattice distortions (defects) of the graphitic network [23]. Such distortions can be due, for example, to the presence of edges of graphitic planes, atomic vacancies or oxygenated groups. Upon reduction of GO under the conditions used in this study, there is a rise in the relative intensity of the D band (see Fig. 3), which seems at odds with the idea that reduction should restore graphitic order and electronic conjugation as suggested by the aforementioned increase in conductivity and the appearance of a $\pi \rightarrow \pi^*$ shake-up peak in the high resolution C1s XPS band. We note that an increase in the intensity ratio of the D and G bands (I_D/I_G) has been found in the early stages of graphene oxidation, caused by the gradual increase in the density of the aforementioned defects of the graphitic network [24]. However, such a trend is only observed up to a certain degree of oxidation and for further oxidation (i.e., upon additional introduction of lattice distortions), the I_D/I_G ratio exhibits a decreasing trend [24]. Such behavior can be attributed to the disappearance of the aromatic, electronically conjugated character from a large number of the six-fold rings as a result of extensive oxidation, which would therefore stop contributing to the D band [4, 5]. Because the graphene sheets have been very extensively oxidized in GO, it would not be unexpected that the reduction led, at least at its first stages to an increase in I_D/I_G ratio, since more aromatic rings are becoming available to contribute to the D band. As chemical reduction with even the most effective reductants (e. g., hydrazine or ascorbic acid) is always limited and a significant number of oxygen-containing groups remain [O/C ratio of ~0.08 (Table 1), which should still amount to a large density of lattice distortions], it is not surprising that we only observe an increase in the D band with reduction (Fig. 3).

Inspection of individual sheets by AFM/STM revealed a clear influence of the reduction degree on their morphology. Fig. 4 shows representative tapping mode AFM images of RGO-

N1 and RGO-V supported on HOPG. The measured sheet thickness tends to gradually decrease with reduction degree (see the included profiles), from 0.9-1.1 nm for GO (image not included) to 0.5-0.6 nm for the most extensively reduced samples (RGO-V and RGO-H). To obtain accurate and consistent results, thickness was determined by measuring heights from overlapped sheets, rather than measuring the sheet height relative to the HOPG substrate [25]. From Fig. 4 the sheets appear to be quite similar on the nanometer scale, except for some small protrusions ~0.5 nm high and ~10 nm in diameter seen in the RGO-V sheets.

More detailed images were obtained by STM as shown in Fig. 5, where the nanometer-scale morphological evolution of the samples with reduction can be better appreciated. The low conductivity of RGO-N1 and RGO-N2 sheets required the use of relatively low currents and high voltages for the tunneling parameters. To allow direct comparisons, STM images of all the reduced samples were taken employing similar tunneling parameters. The slightly reduced RGO-N1 sheets display a smooth irregular surface without distinguishable features, whereas the highly reduced samples RGO-V and RGO-H exhibit an almost flat surface decorated with isolated globular protrusions with lateral sizes of 8-15 nm. Atomic scale STM images of samples RGO-N2 and RGO-V are presented in Fig. 6 (the relatively low conductivity of RGO-N1 sheets did not allow attaining atomic resolution). For both samples, locally ordered or structured domains just a few nanometers large can be seen, which tend to be somewhat larger in the case of RGO-V, as well as for sample RGO-V (image not shown).

In the most widely accepted model, GO sheets are thought to be comprised of randomly distributed highly oxidized zones, in which the vast majority of the oxygen functional groups are present, intermingled with some very small (<3 nm), essentially pristine, isolated graphene regions [14, 26]. Because functionalities should be the main source of local

deformation of the sheets, oxidized areas are thought to be highly buckled, while pristine regions should be flatter. Presumably, reduction diminishes the area of the buckled, oxidized regions and increases that of pristine, flat ones, which is in accordance with the observations of Fig. 5: the STM images of the highly reduced RGO-V/RGO-H sheets (Fig. 5d-g) show a clear contrast between flat/pristine areas, which have become relatively abundant and buckled/oxidized ones (globular protrusions). Such a contrast is not observed for the mildly reduced samples RGO-N1 and RGO-N2 (Fig. 5a and b). In the STM images of the intermediately reduced RGO-P sample (Fig. 5c) the differentiation between both kinds of zones starts to become apparent, thus showing a transition between samples reduced to a lower and a higher extent. Furthermore, the expansion of the more pristine and flatter areas should contribute to the decrease in thickness observed with increasing reduction degree.

4. Conclusions

Chemical reduction of GO can be accomplished to different degrees by controlling several experimental parameters, such as the nature and relative amount of reagents or the reaction time. XPS and TPD analysis showed that reduction mainly proceeds by elimination of the most labile functional groups of GO, which are thought to be mostly located on basal plane positions rather than at edges of the graphene sheets. AFM and STM investigations suggested that reduced GO sheets are composed of a random patchwork of buckled oxidized areas and relatively flat, non-oxidized regions. The relative area of the latter increases with the extent of reduction, which leads to an appreciable decrease in the measured thickness of the sheets. Partial restoration of the graphitic lattice with reduction was also confirmed by the observed increases in electrical conductivity and the appearance of a $\pi \rightarrow \pi^*$ shake-up peak in the high resolution C1s XPS band.

Acknowledgements

Financial support from the Spanish MICINN (project MAT2008-05700) is gratefully acknowledged. R.R. and M.J.F.-M. are thankful for the receipt of a pre-doctoral contract (FPU and FPI, respectively) from MICINN. L.G. acknowledges CSIC for the receipt of postdoctoral JAE-Doc contract.

References

[1] Y. Zhu, S. Murali, W. Cai, X. Li, J.W. Suk, J.R. Potts, R.S. Ruoff, Graphene and Graphene Oxide: Synthesis, Properties, and Applications, Adv. Mater. 22 (2010) 3906-3924.

[2] V. Singh, D. Joung, L. Zhai, S. Das, S.I. Khondaker, S. Seal, Graphene based materials: Past, present and future, Prog. Mater. Sci. 56 (2011) 1178-1271.

[3] S. Stankovich, R.D. Piner, X. Chen, N. Wu, S.T. Nguyen, R.S. Ruoff, Stable aqueous dispersions of graphitic nanoplatelets via the reduction of exfoliated graphite oxide in the presence of poly(sodium 4-styrenesulfonate), J. Mater. Chem. 16 (2006) 155-158.

[4] S. Stankovich, D.A. Dikin, R.D. Piner, K.A. Kohlhaas, A. Kleinhammes, Y. Jia, Y. Wu, S.T. Nguyen, R.S. Ruoff, Synthesis of graphene-based nanosheets via chemical reduction of exfoliated graphite oxide, Carbon 45 (2007) 1558-1565.

[5] J.I. Paredes, S. Villar-Rodil, P. Solís-Fernández, A. Martínez-Alonso, J.M.D. Tascón, Atomic Force and Scanning Tunneling Microscopy Imaging of Graphene Nanosheets Derived from Graphite Oxide, Langmuir 25 (2009) 5957-5968.

[6] T. Szabo, O. Berkesi, P. Forgo, K. Josepovits, Y. Sanakis, D. Petridis, I. Dekany, Evolution of Surface Functional Groups in a Series of Progressively Oxidized Graphite Oxides, Chem. Mat. 18 (2006) 2740-2749.

[7] I. Jung, D.A. Dikin, R.D. Piner, R.S. Ruoff, Tunable Electrical Conductivity of Individual Graphene Oxide Sheets Reduced at "Low" Temperatures, Nano Lett. 8 (2008) 4283-4287.

[8] M.J. Fernández-Merino, L. Guardia, J.I. Paredes, S. Villar-Rodil, P. Solís-Fernández, A. Martínez-Alonso, J.M.D. Tascón, Vitamin C Is an Ideal Substitute for Hydrazine in the Reduction of Graphene Oxide Suspensions, J. Phys. Chem. C 114 (2010) 6426-6432.

[9] J.L. Figueiredo, M.F.R. Pereira, M.M.A. Freitas, J.J.M. Órfão, Modification of the surface chemistry of activated carbons, Carbon 37 (1999) 1379-1389.

[10] H. Nishihara, Q.-H. Yang, P.-X. Hou, M. Unno, S. Yamauchi, R. Saito, J.I. Paredes, A. Martínez-Alonso, J.M.D. Tascón, Y. Sato, M. Terauchi, T. Kyotani, A possible buckybowl-like structure of zeolite templated carbon, Carbon 47 (2009) 1220-1230.

[11] D.-Q. Yang, E. Sacher, Carbon 1s X-ray Photoemission Line Shape Analysis of Highly Oriented Pyrolytic Graphite: The Influence of Structural Damage on Peak Asymmetry, Langmuir 22 (2006) 860-862.

[12] S. Biniak, G. Szymanski, J. Siedlewski, A. Swiatkowski, The characterization of activated carbons with oxygen and nitrogen surface groups, Carbon 35 (1997) 1799-1810.

[13] W.S. Hummers, R.E. Offeman, Preparation of Graphitic Oxide, J. Am. Chem. Soc. 80 (1958) 1339-1339.

[14] A. Lerf, H. He, M. Forster, J. Klinowski, Structure of Graphite Oxide Revisited, J. Phys. Chem. B 102 (1998) 4477-4482.

[15] W. Cai, R.D. Piner, F.J. Stadermann, S. Park, M.A. Shaibat, Y. Ishii, D. Yang, A. Velamakanni, S.J. An, M. Stoller, J. An, D. Chen, R.S. Ruoff, Synthesis and Solid-State NMR Structural Characterization of 13C-Labeled Graphite Oxide, Science 321 (2008) 1815-1817.

[16] A. Ganguly, S. Sharma, P. Papakonstantinou, J. Hamilton, Probing the Thermal Deoxygenation of Graphene Oxide Using High-Resolution In Situ X-ray-Based Spectroscopies, J. Phys. Chem. C 115 (2011) 17009-17019.

[17] D.T. Clark, B.J. Cromarty, A. Dilks, A theoretical investigation of molecular core binding and relaxation energies in a series of oxygen-containing organic molecules of interest in the study of surface oxidation of polymers, J. Polym. Sci. Polym. Chem. Ed. 16 (1978) 3173-3184.

[18] D. Rosenthal, M. Ruta, R. Schlögl, L. Kiwi-Minsker, Combined XPS and TPD study of oxygen-functionalized carbon nanofibers grown on sintered metal fibers, Carbon 48 (2010) 1835-1843.

[19] X. Gao, J. Jang, S. Nagase, Hydrazine and Thermal Reduction of Graphene Oxide: Reaction Mechanisms, Product Structures, and Reaction Design, J. Phys. Chem. C 114 (2010) 832-842.

[20] I. Jung, D.A. Field, N.J. Clark, Y.W. Zhu, D.X. Yang, R.D. Piner, S. Stankovich, D.A. Dikin, H. Geisler, C.A. Ventrice, R.S. Ruoff, Reduction Kinetics of Graphene Oxide Determined by Electrical Transport Measurements and Temperature Programmed Desorption, J. Phys. Chem. C 113 (2009) 18480-18486.

[21] U. Zielke, K.J. Huttinger, W.P. Hoffman, Surface-oxidized carbon fibers: I. Surface structure and chemistry, Carbon 34 (1996) 983-998.

[22] A. Bagri, C. Mattevi, M. Acik, Y.J. Chabal, M. Chhowalla, V.B. Shenoy, Structural evolution during the reduction of chemically derived graphene oxide, Nat. Chem. 2 (2010) 581-587.

[23] A.C. Ferrari, J. Robertson, Interpretation of Raman spectra of disordered and amorphous carbon, Phys. Rev. B 61 (2000) 14095-14107.

[24] D.C. Kim, D.Y. Jeon, H.J. Chung, Y. Woo, J.K. Shin, S. Seo, The structural and electrical evolution of graphene by oxygen plasma-induced disorder, Nanotechnology 20 (2009) 375703.

[25] P. Solís-Fernández, J.I. Paredes, S. Villar-Rodil, A. Martínez-Alonso, J.M.D. Tascón, Determining the thickness of chemically modified graphenes by scanning probe microscopy, Carbon 48 (2010) 2657-2660.

[26] K. Erickson, R. Erni, Z. Lee, N. Alem, W. Gannett, A. Zettl, Determination of the Local Chemical Structure of Graphene Oxide and Reduced Graphene Oxide, Adv. Mater. 22 (2010) 4467-4472.

Table 1. O/C and N/C atomic ratios obtained from XPS survey spectra and total amount of released species obtained by integration of the TPD profiles. For the H_2O column, the first value was obtained by integration over the whole temperature range, so that it includes humidity (adsorbed water); the second value is a guess of the amount of water not coming from humidity calculated by integration in a temperature range above 150 º C.

Sample	Atomic ratios by XPS		Species released by TPD (μmol g^{-1})		
	O/C	N/C	CO	CO_2	H_2O
GO	0.43	0.02	8331	6134	854/~630
RGO-N1	0.30	0.04	2014	4415	469/~293
RGO-P	0.17	0.05	2113	3445	283/~205
RGO-V	0.08	0.01	2071	1827	225/~166
RGO-H	0.08	0.02	1407	1890	66/~45

Figure 1

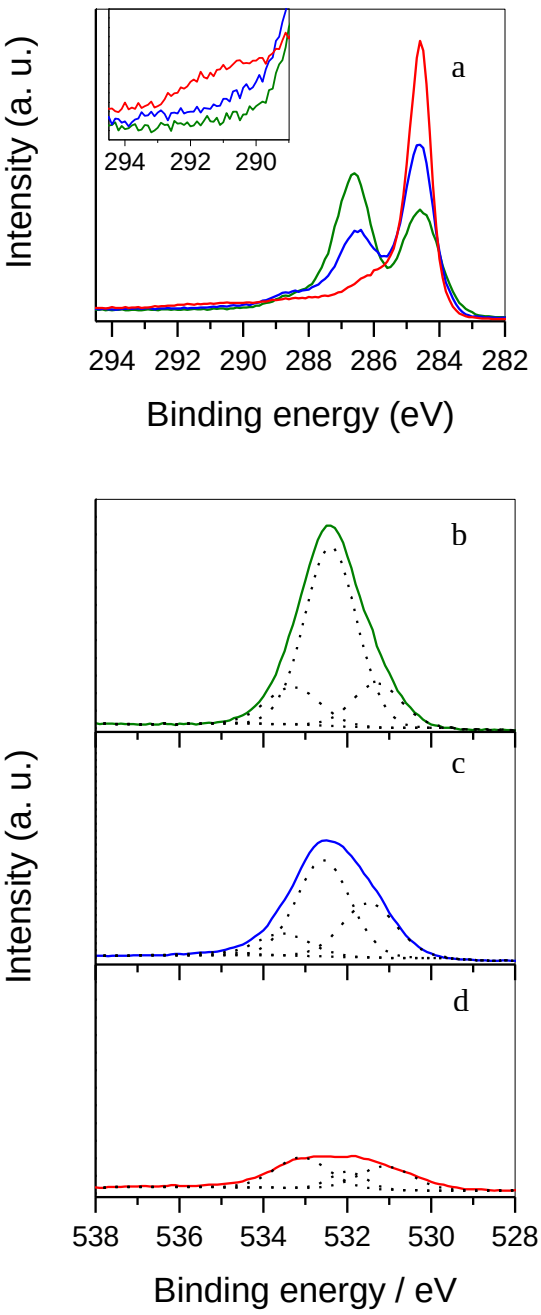
Intensity (a. u.)
a
294 292 290
294 292 290 288 286 284 282
Binding energy (eV)
b
c
d
538 536 534 532 530 528
Binding energy / eV

Figure 2

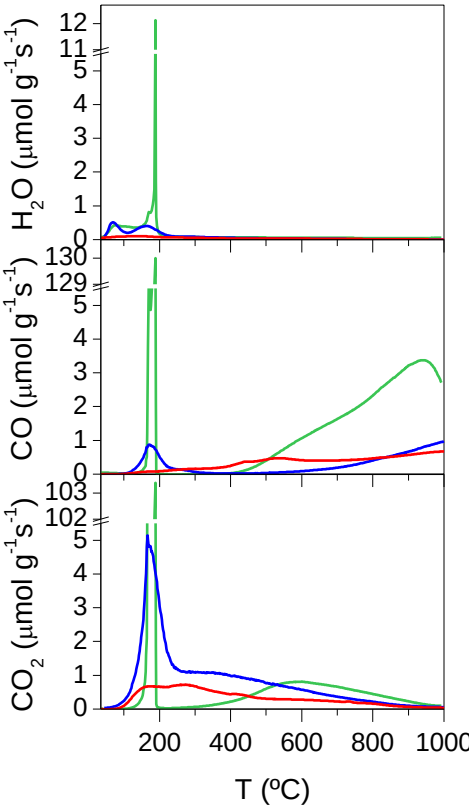
H2O (μmol g-1s-1)
CO (μmol g-1s-1)
CO2 (μmol g-1s-1)
T (ºC)
200
400
600
800
1000

Figure 3

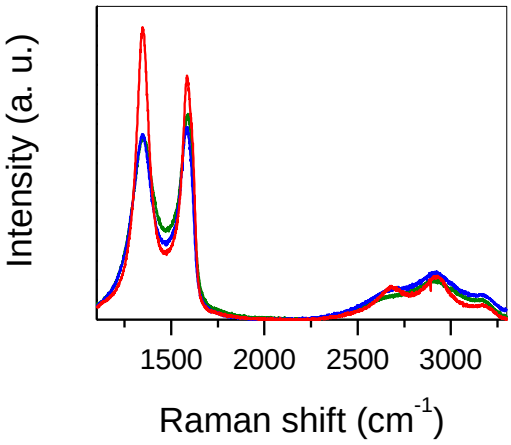

Figure 4

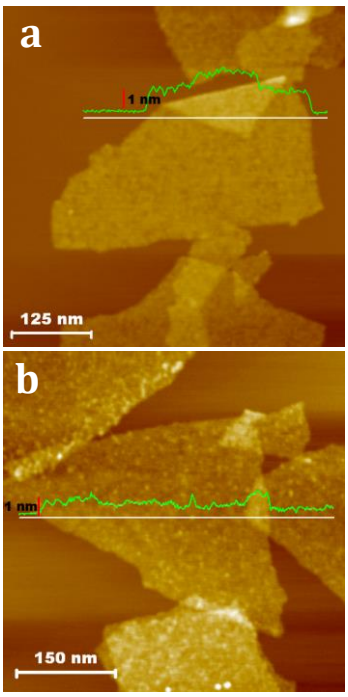

Figure 5

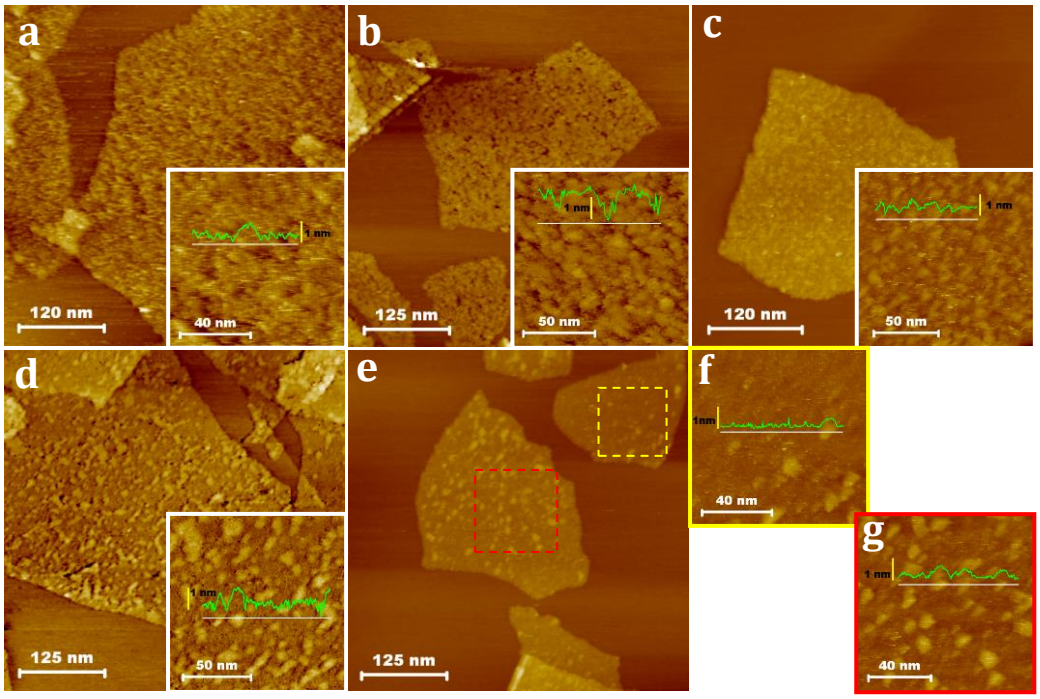
a
120 nm
1 nm
40 nm
b
125 nm
1 nm
50 nm
c
120 nm
1 nm
50 nm
d
125 nm
1 nm
50 nm
e
125 nm
f
1 nm
40 nm
g
1 nm
40 nm

Figure 6

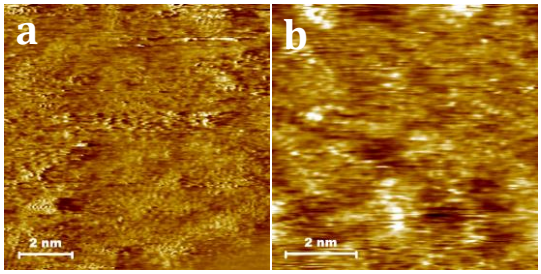

Captions to Figures

Figure 1. High resolution C1s (a) and O1s (b-d) core level XPS spectra of GO (green), RGO-N1 (blue), and RGO-V (red). The spectra in (a) are normalized and a magnification of the higher binding energy range is shown in the inset.

Figure 2. From top to bottom, TPD profiles for the samples GO (green), RGO-N1 (blue), and RGO-V (red) for H_2O, CO, and CO_2.

Figure 3. Normalized Raman spectra of GO (green), RGO-N1 (blue), and RGO-V (red)

Figure 4. Tapping mode AFM images of (a) RGO-N1 and (b) RGO-V sheets, with included line profiles.

Figure 5. STM images of (a) RGO-N1 (75 pA, 2000 mV), (b) RGO-N2 (inset: 200 pA, 500 mV), (c) RGO-P , (d) RGO-V , and (e-g) RGO-H with insets showing more detailed areas. The tunneling parameters employed to collect these images were 250 pA and 1000 mV, except for the cases indicated in the parentheses.

Figure 6. Atomic scale STM images of (a) RGO-N2 (2.5 nA, 10 mV) and (b) RGO-V (3.5 nA, 3 mV).